catalysts

MDPI

Article

Modeling of a Two-Bed Reactor for Low-Temperature Removal of Nitrogen Oxides in Nitric Acid Production

Nadezhda Vernikovskaya *, Yuliya Ivanova, Artem Sheboltasov, Victor Chumachenko * and Lyubov Isupova

Boreskov Institute of Catalysis, pr. Lavrentieva, 5, Novosibirsk 630090, Russia
* Correspondence: vernik@catalysis.ru (N.V.); vachum@catalysis.ru (V.C.)

Abstract: In this study, the modeling of the low-temperature catalytic abatement of NO_X and N_2O from tail gases in a weak nitric acid plant utilizing a single-pressure 0.716 MPa system was performed. A one-reactor concept assumes that in the first bed, NO_X is reduced by ammonia on a commercial vanadia–alumina catalyst, and in the second bed, N_2O is decomposed on a proprietary nickel–cobalt catalyst. The kinetics of N_2O decomposition on a $Cs/Ni_{0.1}Co_{2.9}O_4$ catalyst was experimentally studied in an isothermal flow reactor. The reaction rate constants were determined by varying the residence time and temperature; these data formed the basis for modeling kinetics and heat and mass transport in an adiabatic reactor in which the low-temperature mitigation of nitrogen oxides occurred. Taking into account the given spatial limitations inside the reactor and the allowable temperatures, the layer heights were evaluated to ensure a residual NO_X and N_2O content of less than 50 ppm. Catalyst loading using layers in a commercial reactor was estimated for the tail-gas flow rates of 46,040–58,670 m^3/h. Simulations showed that the optimum inlet temperature was 260 °C; in this case, the NO_X and N_2O conversion targets were achieved in the range of 46,040–58,670 m^3/h while adhering to catalyst bed height and outlet temperature limitations.

Keywords: $Cs/Ni0.1Co_{2.9}O_4$ catalyst; de-N_2O; one-reactor concept; kinetic modeling; mathematical modeling

Citation: Vernikovskaya, N.; Ivanova, Y.; Sheboltasov, A.; Chumachenko, V.; Isupova, L. Modeling of a Two-Bed Reactor for Low-Temperature Removal of Nitrogen Oxides in Nitric Acid Production. *Catalysts* **2023**, *13*, 535. https://doi.org/10.3390/catal13030535

Academic Editors: Maria Jaworska and Piotr Lodowski

Received: 22 January 2023
Revised: 28 February 2023
Accepted: 2 March 2023
Published: 6 March 2023

1. Introduction

Capturing greenhouse gases is one of the greatest technological challenges. Of these GHGs, nitrous oxide (N_2O) has 310 times more global warming potential than CO_2. Human activities such as agriculture, fuel combustion, wastewater management, and industrial processes are increasing the amount of N_2O in the atmosphere. Globally, about 40% of total N_2O emissions come from anthropogenic sources. Stimulated by the need for fertilizers, the production of nitric acid results in N_2O emissions that can be reduced through technological upgrades and the use of abatement equipment. In nitric acid production, N_2O emissions are estimated at 300,000–400,000 t/year [1]. The emission of N_2O exclusively depends on the ammonia combustion process. Once formed, N_2O passes unreacted through the plant and is not affected by the operating conditions. In weak nitric acid production, all known approaches to N_2O reduction can be classified into several groups, according to their ranking in terms of the technological process. The most widely used are the primary, secondary, and tertiary systems for N_2O abatement. The primary methods consist of the optimization of the composition of a platinoid gauze pack and operating conditions of an ammonia burner, aimed at the formation of free volumes for the homogeneous decomposition of nitrous oxide at high temperatures. This results in the suppression of the N_2O formation during the oxidation of NH_3 and the interaction of the reaction products with the "leaked" ammonia. The secondary methods assume the decomposition of nitrous oxide on the catalyst installed in the hot zone immediately downstream of the gauze packs. Yara, BASF, J. Matthey, and Heraeus have proposed high-temperature ceramic-supported catalysts based on precious metals or metal oxides [2]. Tertiary abatement measures ensure

the removal of N_2O in the tail gas (the stream leaving the absorber) via direct catalytic decomposition (de-N_2O process) (Table 1). They have great advantages, as they do not affect the other elements of the nitric acid production process and can be applied in several variants [3]. In European countries, the N_2O emissions per ton of the produced nitric acid vary considerably, as evidenced by the current guidelines for estimating national N_2O emissions as specified by the internationally recognized IPCC (Intergovernmental Panel on Climate Change) [1]. The N_2O emission factor for HNO_3 production can range from <2 to 19 kg N_2O per ton of 100% HNO_3.

Table 1. Methods of tail-gas purification.

The Purification Method	Temperature, °C	Catalyst	Process	Reactor	Technology Developed by
Non-selective catalytic reduction (reducing agents: H_2, hydrocarbons)	720–770	Pd-containing	de-NO_x de-N_2O	NSCR	GIAP
Selective catalytic reduction (reducing agents: NH_3)	250–520	MnO_2, CuO, Fe_2O_3, Zeolite, V/Al	de-NO_x	SCR	BASF BIC RAS
EnviNO$_x$®	350–520	Zeolite	de-NO_x de-N_2O	EnviNO$_x$	Uhde

Combining two consecutive catalytic beds to remove NO_X and N_2O at close temperatures is in line with the current technological trends and can be accomplished in a single reactor [4]. The layer-by-layer loading of various catalysts is a well-known technique, and it is also used in waste-gas purification processes. For example, it is used in Uhde's EnviNO$_x$®variants of integrated nitrogen oxides (NO_x and N_2O) abatement technology [3]. Several years ago, ThyssenKrupp Industrial Solutions commercialized technologies EnviNO$_x$®for tail-gas purification in a two-bed reactor at medium temperatures [3]. In one version, the catalytic decomposition of N_2O occurs on an iron–zeolite catalyst at 425–520 °C in the first bed; NO_X is catalytically reduced by ammonia to N_2 on a similar catalyst in the second bed. In another version, which is suitable for lower tail-gas temperatures of 300–500 °C, ammonia is injected together with these gases; SCR NO_X with ammonia occurs in the first bed, and N_2O reduction occurs in the second bed after the addition of natural gas or propane.

In Russia, industrial weak nitric acid plants with a capacity of 345 t/day operating at a single pressure of 0.716 MPa (UKL plant) are equipped with reactors for the low-temperature selective catalytic reduction of nitrogen oxides by ammonia from tail gases. The design of the SCR reactor allows for the setup of not only a bed of SCR catalyst, the height of which is ~0.5 m, but also a bed of de-N_2O catalyst up to 0.7 m high. Thus, tail-gas purification can be carried out in a single reactor, by using catalytic beds providing both SCR of NO_x with ammonia and de-N_2O in the temperature range of 250–300 °C [5,6]; the catalyst arrangement options in the adiabatic reactor can vary. However, if the de-N_2O catalyst is placed in the first bed, ammonia must be injected before the second bed, where the de-NO_x catalyst is located. This will require precise ammonia control to eliminate the extra N_2O formation during SCR. Therefore, based on the actual temperature modes for SCR and de-N_2O catalysts, the most rational seems to be the option in which the first bed contains an SCR catalyst (NH_3 is introduced together with tail gases), and the second bed contains an N_2O decomposition catalyst. This option can be readily tailored to the existing industrial reactors. Currently used at UKL plants, the abatement of NO_x by SCR provides NO_x level < 50 ppm, which meets environmental standards. This process is carried out on the aluminum–vanadium catalysts AVK-10 and AOK-78-55 with V_2O_5 content of 12–12.5%, and MnO_2 of 1–1.5% can be added as well. An improved technology made it possible to

reduce the content of vanadium pentoxide to 5–7% [7] from 12–15% [8] while maintaining high activity and selectivity for molecular nitrogen. Usually, V/Al SCR catalysts operate in the temperature range of 220–280 °C without loss of selectivity for N_2. As the gases after SCR contain 0.15% N_2O, 2.5% O_2, and 3% H_2O [5,6], it is essential to use a de-N_2O catalyst, which can work in a close temperature range and in the reaction medium after the SCR catalyst.

The decomposition of N_2O is an irreversible exothermic reaction. It proceeds via two mechanisms: the Langmuir–Hinshelwood (L–H) mechanism characterized by the low activation energy of the stage of surface oxygen diffusion and recombination (stage 1), and the Eley–Rideal (E–R) mechanism characterized by the high activation energy of surface diffusion, which requires large amounts of energy for oxygen diffusion (stage 3) [9–11]:

$$N_2O + S \rightarrow N_2\uparrow + S \ldots \text{Osurf} \quad (1)$$

$$2\,S \ldots \text{Osurf} \leftrightarrow 2S + O_2\uparrow \text{(L-H)}, \quad (2)$$

$$2\,S \ldots \text{Osurf} + N_2O \rightarrow 2\,S + O_2\uparrow + N_2\uparrow \text{(E-R)}, \quad (3)$$

where S is the active site of the surface, and S . . . O surf is the oxygen adsorbed on the active site of the surface. For various oxide systems, stages (2) and (3) were found to be relatively slow compared with stage (1). In other words, O_2 desorption can be considered the rate-determining stage of the catalytic decomposition of N_2O regardless of the mechanism of O_2 formation. Thus, the kinetics of de-N_2O depends on temperature, pressure, and the competitive adsorption of inhibitors (O_2 and H_2O) on active sites.

A variety of catalytic systems for the low-temperature decomposition of N_2O includes [12,13] platinum-group metals (Ru, Rh, Pd, Ir, and Pt), oxides of rare-earth elements, and oxides of transition d-elements (in particular, Cu, Ni, Co, and Fe) [14–18]. Many catalytic systems containing noble metals and elements of the rare-earth subgroup are deactivated in the presence of inhibitors and have a high cost, which makes it difficult to use them as catalysts for exhaust-gas purification. To date, the spinel-like structure of Co_3O_4 oxide, as well as the binary substituted oxides based on it, have proved to be the most promising candidates for de-N_2O due to the redox ability of cobalt, a high concentration of oxygen vacancies, and a weak Co-O bond [19,20]. The substitution of Co atoms in certain positions of the spinel oxide matrix has a significant effect on the binding energy of the active center with oxygen. Magnesium and nickel substituted by Co_2O_3 spinels demonstrated the highest activity in the reaction of N_2O decomposition. The incorporation of Ni^{2+} or Mg^{2}+ into the Co_3O_4 structure promotes better desorption of O_2 and lowers the temperature of de-N_2O [21–26]. Both cations can displace cobalt not only in the tetrahedral environment but also to some extent in the octahedral one [27]. This leads to structural distortions with an increase in the bond lengths in octahedra and a decrease in tetrahedra. The effect is more pronounced for nickel-substituted Co_3O_4 spinels and to a lesser extent for magnesium-substituted ones. The modification of Co_3O_4 spinels with alkali metal cations makes them more active and resistant to inhibitors [28,29]. The beneficial effect of different alkali promoters on the Co_3O_4 activity in nitrous oxide decomposition increases in the following order: Li $\ll$ Na < Rb $\cong$ K < Cs [28,29]. This is consistent with a decrease in the electronegativity values from Li to Cs [30]. Most studies on the effect of the nature of the alkaline modifier and its precursors were mainly conducted for pure Co_3O_4 spinels.

The catalysts based on Ni(Mg)-substituted cobalt spinels modified with alkali metals $Cs/Ni(Mg)_xCo_{3-x}O_4$ [9,31,32] are promising for low-temperature N_2O decomposition as second-bed catalysts in the abatement of NO_x and N_2O from tail gases [5,31].

The main novelty of this paper lies in presenting a single-reactor concept with the low-temperature catalytic control of NO_x and N_2O from the tail gases emitted at weak nitric acid plants. In the first bed, NO_x is reduced by ammonia, and in the second bed, N_2O is decomposed on a proprietary catalyst. More than half of the industrial plants producing nitric acid in Russia utilize a low-temperature V–Al catalyst to remove NO_X emissions using SCR. Under such conditions, a low-temperature N_2O decomposition catalyst is required. A

new $Cs/Ni_{0.1}Co_{2.9}O_4$ catalyst for the decomposition of nitrous oxide at low temperatures is also another new aspect of this paper.

The main objective of this study is to determine the conditions for the combined low-temperature catalytic purification of NO_x and N_2O from the tail gases of weak nitric acid plants, providing NO_x and N_2O removal rates of at least 98%, i.e., to no more than 50 ppm, in a single two-bed reactor. It is assumed that a commercially available vanadium–aluminum catalyst [6–8] is used for the SCR of NO_X, and a new $Cs/Ni_{0.1}Co_{2.9}O_4$ catalyst is used for the low-temperature decomposition of N_2O [9,33]. The following restrictions should be taken into account:

- The catalyst bed height should not exceed the maximum allowable space according to the UKL plant's catalytic purification reactor design: 0.5 m for SCR and 0.7 m for de-N_2O;
- The maximum temperature in the SCR catalyst bed should not exceed 280 °C because the selectivity of vanadium–aluminum catalysts decreases at a higher temperature.

2. Results and Discussion

2.1. Kinetic Modeling

The experimental data obtained in the isothermal flow reactor and plotted in Figure 1 (symbols) demonstrate that the proper choice of residence time and reaction temperature makes it possible to achieve a high nitrous oxide conversion efficiency, in the range of 95–99% even at moderate temperatures. The highest degree of N_2O conversion was obtained at 250–280 °C. The stable operation of the catalyst was maintained for at least 2 h.

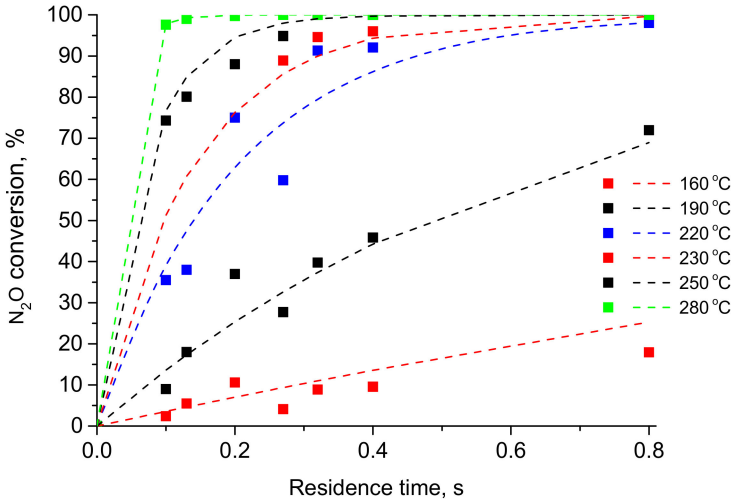

Figure 1. Conversion of N_2O on Cs/Ni-Co oxide catalyst vs. residence time at different temperatures. Symbols indicate the experimental data. Lines indicate the results of modeling based on estimated parameters.

The evaluated values of the pre-exponential factor (k_0) and the activation energy (E_a) of the de-N_2O reaction rate constant (k) were found to be $7.23 \cdot 10^8$ s^{-1} and 77.15 kJ/mol, respectively (Table 2). The results of modeling based on the estimated parameters are plotted in Figure 3 (lines).

Table 2. Kinetic constants for de-N_2O reaction.

Kinetic Parameters		Confidence (+/−)	
k_0, s^{-1}	E_a, J/mol	k_0, s^{-1}	E_a, J/mol
$7.23 \cdot 10^8$	77,150	$0.37 \cdot 10^8$	3360

2.2. Process Modeling

The calculations showed that an increase in the flow rate of gas entering the reactor reduced the residence time (τ) in the catalyst bed, which led to a decrease in the conversion of nitrogen oxides (X). To increase τ, it is necessary to increase the height of the catalyst bed, but in this case, the H_{max} limitation could not be met.

At T_g^{in} = 230–240 °C, the height of the second bed significantly exceeded 0.7 m for all the Q values from the considered range. An increase in T_g^{in} led to an increase in the reaction rate, which made it possible to achieve the required conversion at a lower H. Since SCR and de-N_2O reactions are exothermic, the temperature increased along the height of each layer. The maximum adiabatic temperature rise (ΔT_{ad}) in the first layer at the required conversion of the initial amount of NO_x was approximately 20 degrees and in the second layer at the required conversion of N_2O—4.04 degrees. The temperature at the outlet of the first bed was equal to $T_g^{in} + \Delta T ad_1$, and at T_g^{in} = 270 °C, it became higher than the permissible value of 280 °C.

The conversion and temperature profiles along the bed heights at the maximum gas flow rate of Q = 58,670 m^3/h and T_g^{in} = 250 °C are presented in Figure 2. The temperature of 270 °C at the outlet of the first bed was within the temperature limit T_{max}. However, under these conditions, the height of the first bed was 0.52 m, and the height of the second bed was 0.79 m; thus, the heights of both these layers exceeded the permissible values.

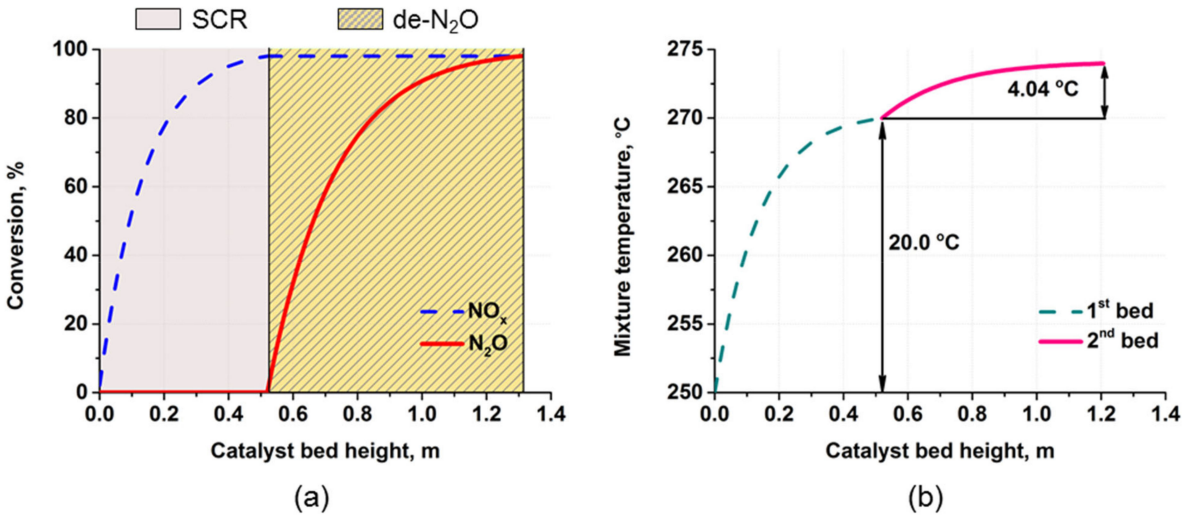

Figure 2. Conversion (**a**) and temperature (**b**) profiles along the bed heights at T_g^{in} = 250 °C and Q = 58,670 m^3/h.

At the fixed T_g^{in} = 250 °C, if Q decreased (i.e., the residence time τ increased), the bed height required to achieve a given conversion rate decreased (Figure 3, solid lines). With $Q \leq$ 52,000 m^3/h, the height of each bed was within the specified limits, and T_{max} did not exceed 280 °C.

Figure 4 shows the NO_x and N_2O conversion and temperature profiles along the beds at T_g^{in} = 270 °C and Q = 58,670 m^3/h. A higher inlet temperature contributed to a much lower bed height for any Q, which allowed the specified limits to be reached. However, the outlet temperature in the first bed considerably exceeded the limit of 280 °C for all Q values (Figure 3, dash-dotted lines), which is unacceptable for an SCR catalyst. Therefore, the implementation of the process at T_g^{in} = 270 °C was not possible.

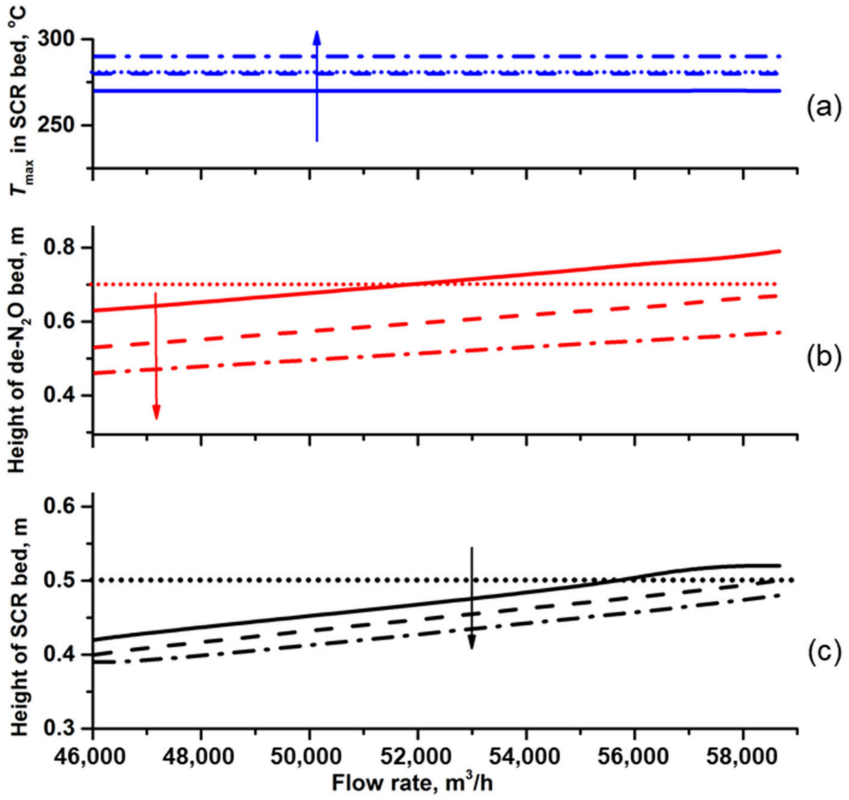

Figure 3. Maximum temperature (**a**), height of de-N_2O bed (**b**), and height of SCR bed (**c**) vs. flow rate. T_g^{in} = 250 °C (solid lines), 260 °C (dashed lines), and 270 °C (dash-dotted lines). The dotted lines show the maximum allowable values. The arrows indicate increasing T_g^{in}.

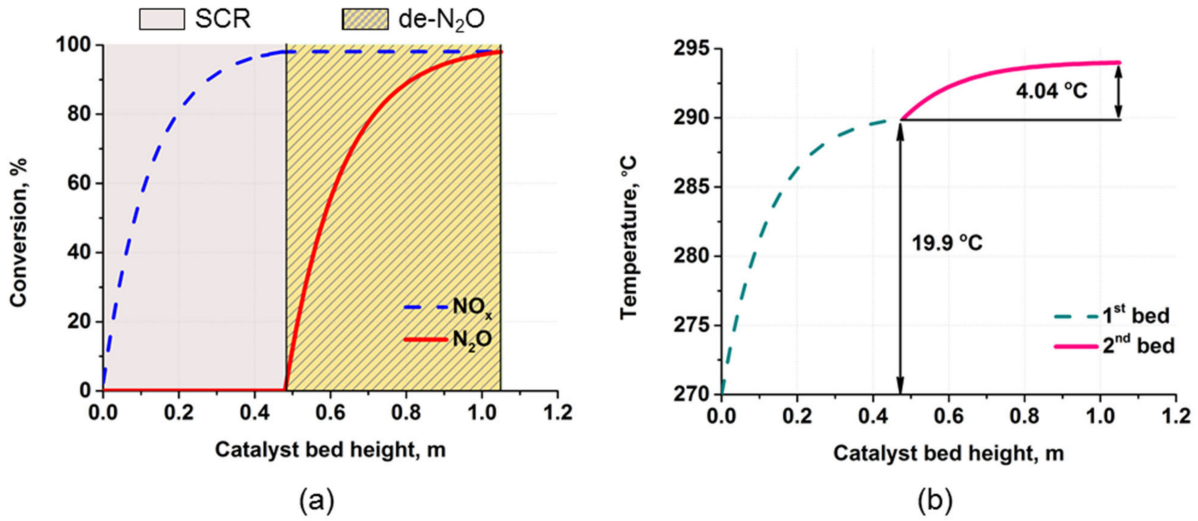

Figure 4. Conversion (**a**) and temperature (**b**) profiles along the bed heights at T_g^{in} = 270 °C and Q = 58,670 m^3/h.

At T_g^{in} = 260°C, the bed heights also became lower, but the maximum temperatures did not exceed the specified limits. For all the Q values from the considered range, the limits for the allowable height of the first and second catalyst bed were determined (Figure 5, dashed lines).

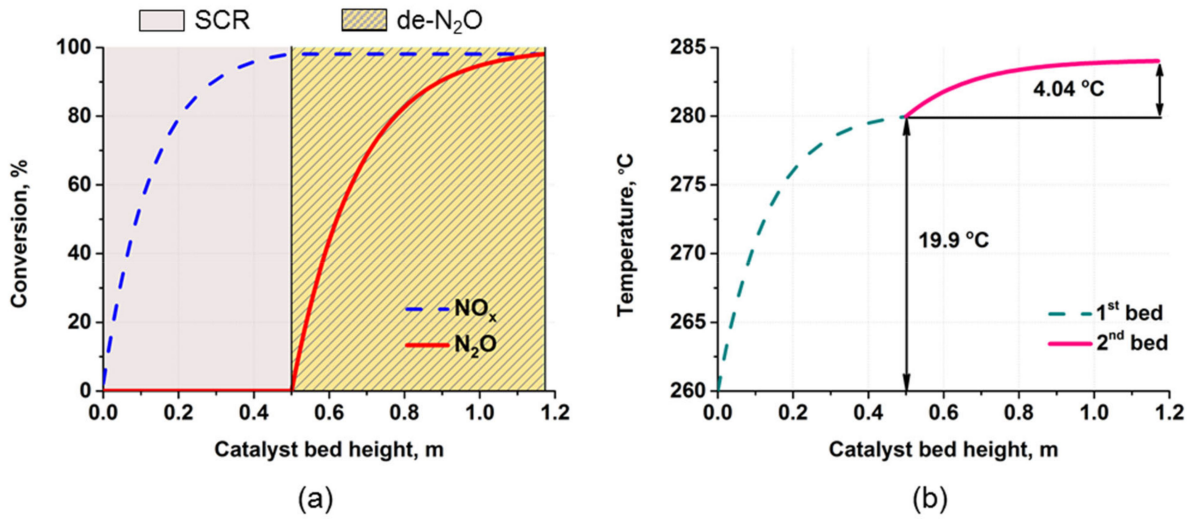

Figure 5. Conversion (**a**) and temperature (**b**) profiles along the bed heights at T_g^{in} = 260 °C and Q = 58,670 m^3/h.

The simulation results at T_g^{in} = 260 °C and the maximum gas flow rate Q = 58,670 m^3/h are shown in Figure 5. The temperature at the SCR bed outlet was 279.9 °C. The calculated bed height was 0.5 m for the SCR catalyst and 0.67 m for the de-N_2O catalyst, which satisfied all the given limitations.

Thus, the mathematical modeling of catalytic NO_x and N_2O abatement from tail gas demonstrated that when the temperature of the tail gas was T_g^{in} = 250 °C, the process provided an acceptable residual content of NO_x and N_2O if the flow rate of the tail gas was $Q \leq$ 52,000 m^3/h, and at T_g^{in} = 260 °C, for all the Q values from the considered range. The restrictions of the bed heights in the adiabatic reactor and the maximum temperature restrictions in the SCR bed were met for both options. The hydraulic resistance of the beds and the weight of catalysts are given in Table 3.

Table 3. The bed heights, the total pressure drop along the beds, and catalyst loading.

T_g^{in}, °C	Bed	Q, m^3/h (STP)	H, m	ΔP *, kPa	G, tons
250	SCR	46,040	0.42	3.01	4.29
	de-N_2O		0.63	6.87	6.43
	SCR	47,038	0.43	3.20	4.39
	DeN_2O		0.64	7.25	6.53
260	SCR	46,040	0.40	2.92	4.08
	de-N_2O		0.53	5.89	5.41
	SCR	47,038	0.41	3.11	4.18
	de-N_2O		0.54	6.23	5.51
	SCR	55,035	0.47	4.78	4.80
	de-N_2O		0.63	9.68	6.43
	SCR	56,400	0.48	5.11	4.90
	de-N_2O		0.64	10.27	6.53
	SCR	57,600	0.49	5.43	5.00
	de-N_2O		0.66	11.02	6.74
	SCR	58,670	0.50	5.73	5.10
	de-N_2O		0.67	11.57	6.84

* Calculated at 1 atm.

For a rough comparison of the simulation results with the literature data, we used the data given in [34] when calculating the N_2O decomposition reactor at 450 °C on a cobalt-containing catalyst (Co-Mg-Al, K-promoted) in the form of 3 × 3 mm extrudates. To achieve the target conversion rate of 90% (100 ppm N_2O residual) at a flow rate of 30,000 m^3/h (STP), 11.5 m^3 (ca. 15 tons) of catalyst was required, with a pressure drop of 20 kPa over the catalyst bed. As can be seen from Table 6, a smaller catalyst volume (up to 8 m^3) and a pressure drop (up to 12 kPa) were required to destroy 1500 ppm N_2O to a residual 50 ppm; hence, the catalyst weight and hydraulic resistance of the bed were less than those for a similar reactor.

When the process was run at T_g^{in} = 250 °C and Q = 46,040–47,038 m^3/h, the pressure drop did not exceed 9.9–10.5 kPa, and the total catalyst weight was 10.7–10.9 tons (Table 3). At T_g^{in} = 260 °C and Q = 46,040–58,670 m^3/h, ΔP was in the range of 8.8–17.3 kPa, and G was 9.5–11.9 ton (Table 6). It should be emphasized that with a flow rate of ~46,000–47,000 m^3/h, the process operation at 260 °C can slightly save the catalyst load and pressure drop compared with the variant at T_g^{in} = 250 °C. In a wider range of flow rates, an inlet temperature of 260 °C can be regarded as the optimal value to ensure high abatement performance, no catalyst overheating, low-pressure drop, and catalyst loading.

The combination of a NO_x SCR catalyst and a N_2O decomposition catalyst in one reactor is very attractive. This approach does not require considerable engineering and reconstruction work for the existing plants equipped with low-temperature SCR de-NO_x technology. There are about 100 industrial nitric acid plants in Russia, more than half of which use low-temperature V–Al catalysts to remove NO_x using SCR from the tail gas and are the main source of nitrous oxide emissions. Under such conditions, traditional high-temperature catalysts for the decomposition of N_2O (iron-containing zeolites) would require additional gas heating, which is not economically feasible. The use of a combined tail-gas cleaning system with a low-temperature N_2O decomposition catalyst makes it possible to reduce the energy costs for tail-gas heating and avoid CO_2 emissions, which is inevitable during high-temperature nonselective N_2O reduction with hydrocarbons. To protect the environment from the harmful effects of N_2O emissions, the development of a combined NO_x + N_2O abatement system is useful and relevant.

3. Experimental

Through the co-precipitation of the aqueous solutions of $Co(NO_3)_2 \cdot 6H_2O$ (REAHIM, Moscow, Russia) and $Ni(NO_3)_2 \cdot 6H_2O$ (REAHIM, Moscow, Russia) salts, a substituted cobalt spinel $Ni_xCo_{3-x}O_4$ with a molar degree of substitution x = 0.1 was obtained. Precipitation was performed at room temperature, and pH = 8–8.5; $(NH_4)_2CO_3$ (REAHIM, Moscow, Russia) was used as a precipitant. The precipitate was filtered off, washed to pH = 7, and dried for 10 h at a temperature of 120 °C. The dry precipitate was modified via impregnation with 2 wt% cesium ($CsNO_3$ solution) (REAHIM, Moscow, Russia). Ethylene glycol and citric acid were added to the impregnating solution containing cesium nitrate (the Pechini method). After calcination for 2 h at 450 °C, a 2% $Cs/Ni_{0.1}Co_{2.9}O_4$ (Cs/Ni-Co) sample was obtained. All chemicals were 99.9% pure (purissimum).

The phase composition of the sample was determined using X-ray phase analysis (XRD) on a Bruker D8 diffractometer (Karlsruhe, Germany) using CuK_α radiation (λ = 1.5418 Å).

The sample was scanned point by point with an interval of 0.05° in the 2θ range from 10 to 70°. Figure 6 shows that the X-ray pattern of the sample corresponds to the spinel phase. The structural parameters were calculated using the FullProff program (a = b = c = 8.088 Å). The size of the coherent scattering region (CSR~260 Å) was determined using the Selyakov–Scherer formula. The specific surface area of the sample (S_{sp} = 32 m^2/g) was measured through argon sorption at 77K, followed by thermal desorption, at four points of the sorption equilibrium with a SORBI-M 4.1 instrument (ZAO META, Novosibirsk, Russia) using the SORBI-M Version 4.2 software. Helium was used as a carrier gas. Specific surface area values were calculated using the BET method. High-pressure mercury porosimetry

with an AutoPore IV 9500 V1.09 instrument (Micromeritics, Norcross, GA, USA) was used for studying the porous structure of the catalyst (the median pore diameter of the sample was 0.03 μm).

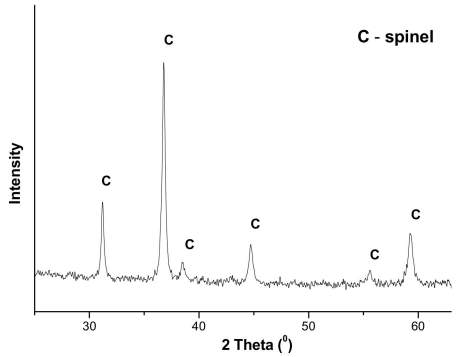

Figure 6. XRD patterns of Cs/Ni-Co sample.

In kinetic experiments, the activity was determined on a laboratory setup (Figure 7) with an isothermal flow reactor in the flow rates range of 5.4–1.8 l/h (residence time 0.27–0.8 s); the catalyst was tested as a 0.25–0.50 mm fraction with the following reaction mixture at the inlet: 1500 ppm N_2O, 2.5% O_2, ~3% H_2O, and He balance. The kinetic experiments were carried out at atmospheric pressure (an increase of 0.01 atm was allowed). The N_2O concentration at the reactor inlet and outlet was determined online at 120 °C using an FT-801 FT-IR spectrometer (Simex, Novosibirsk, Russia).

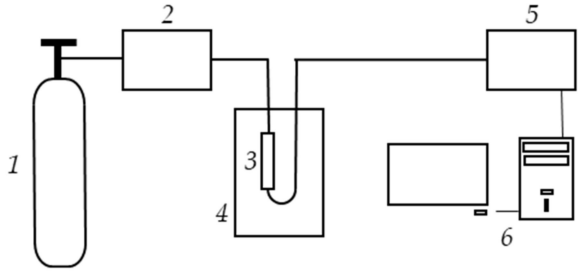

Figure 7. The laboratory setup diagram: *1*—cylinder; *2*—gas-flow-rate controller; *3*—reactor with the catalyst; *4*—furnace; *5*—FT-801 Fourier transform IR spectrometer; *6*—data-processing unit.

4. Mathematical Model

4.1. Description of the Reaction System and Governing Equations of the Model

Mathematical modeling is an effective tool for predicting the conditions that ensure the highest catalyst performance in the low-temperature purification of tail gases from nitrogen oxides in adiabatic reactors. This will contribute to the optimization of operating expenses during the practical implementation of the proposed single-reactor concept at UKL plants.

When formulating the mathematical model, it should be taken into account that the adiabatic fixed-bed reactor under consideration has a thermally insulated wall to minimize heat losses, and the catalytic beds feature a large diameter-to-height ratio. Therefore, radial heat and mass transfers have no significant influence and can be neglected in the model, but it is important to consider the conductive heat transfer and diffusive mass transfer in the axial direction.

To provide the necessary residence time at a bed height of 0.5–0.7 m, the linear gas velocity in the reactor should not exceed 1.0–1.5 m/s. At such linear velocities, the interphase heat and mass transfers between the catalyst and the gas can affect the performance of the catalyst [35–37]. Thus, to simulate the NO_x and N_2O abatement process in an adiabatic

two-bed reactor, we used a stationary two-phase mathematical model for each catalytic bed that took into account the following factors:

- Convective heat and mass transfers in the gas phase;
- Axial diffusion in the gas phase;
- Axial heat transfer due to thermal conductivity in the solid phase;
- Interphase heat and mass transfers;
- Chemical reactions (SCR of NO_x with ammonia in the first bed, N_2O decomposition in the second bed);
- Heat release as a result of exothermic reactions in the solid phase.

4.2. Governing Equations of the Model

The mass and energy balance equations and the boundary conditions for each bed of the adiabatic reactor are given in Table 4. In the first bed, the reaction of SCR NO_x with ammonia proceeds at a rate of W_{SCR} and enthalpy ($-\Delta H_{SCR}$), while in the second bed, the reaction of de-N_2O proceeds at a rate of W_{N_2O} and enthalpy ($-\Delta H_{N_2O}$). At the inlet to the first bed, the inlet values of species concentrations y_{gi}^{in} and temperature T_g^{in} are set. At the inlet to the second bed, the species concentrations after the first bed are taken as inlet values y_{gi}^{in}, and the temperature at the outlet from the first bed is taken as T_g^{in}.

For calculating model parameters, we used the correlations given in Table 5.

Table 6 shows the catalyst dimensions, stoichiometric equations, enthalpies, and kinetic equations for SCR NO_x via ammonia and de-N_2O reactions. In [31], it was shown that the reaction rate of SCR NO_x using ammonia on a V_2O_5/Al_2O_3 catalyst can be determined using a first-order kinetic equation with respect to NO_x. The kinetic constants (k_0 = 252.1 s^{-1} and E_a = 13,390 J/mol) correspond to the observed reaction rate of the SCR of nitrogen oxides with ammonia on catalyst granules in the form of cylinders 5 × 15 mm [44]. In [31,45,46], it was shown that the reaction rate of the nitrous oxide decomposition on oxide Ni/Co-containing catalysts can be determined using a first-order equation with respect to N_2O. The effectiveness factor and the observed reaction rate of N_2O decomposition for the catalyst granules with a diameter of 3.4 mm were calculated during the simulation using Equations (13) and (14) (Table 5).

Table 4. The stationary non-isothermal mathematical model of the catalytic process in adiabatic reactor.

Balance Equation	Boundary Conditions
Mass balance	
Gas phase	
$-u_0\frac{\partial y_{gi}}{\partial z}+\frac{\partial}{\partial z}\left(\frac{P}{T_g}\cdot\frac{T_0}{P_0}\cdot D_i^e\frac{\partial y_{gi}}{\partial z}\right)+S_{sp}\cdot\beta_i\cdot\frac{P}{T_g}\cdot\frac{T_0}{P_0}\cdot\left(y_{ci}-y_{gi}\right)=0,\ i=1,N$ (4)	$z=0:\frac{P}{T_g}\cdot\frac{T_0}{P_0}\cdot D_i^e\frac{\partial y_{gi}}{\partial z}=u_0\left(y_{gi}^{in}-y_{gi}\right);$ (8)
Solid phase	$z=H:\frac{\partial y_{gi}}{\partial z}=0.$ (9)
$-S_{sp}\cdot\beta_i\cdot\frac{P}{T_g}\cdot\frac{T_0}{P_0}\cdot\left(y_{ci}-y_{gi}\right)+\nu_i\cdot V_m\cdot W=0,\ i=1,N$ (5)	
Energy balance	
Gas phase	
$c_p\left(T_{ref}\right)\frac{u_0}{V_m}\frac{\partial T_g}{\partial z}=S_{sp}\cdot\alpha\cdot\left(T_c-T_g\right)$ (6)	$z=0:T_g=T_g^{in},\ \frac{\partial T_c}{\partial z}=0;$ (10)
Solid phase	$z=H:\frac{\partial T_c}{\partial z}=0.$ (11)
$-\frac{\partial}{\partial z}\left(\lambda^e\frac{\partial T_c}{\partial z}\right)=S_{sp}\cdot\alpha\cdot\left(T_c-T_g\right)+(-\Delta H)\cdot W$ (7)	

Table 5. Correlations for calculating model parameters.

Parameter	Equation		Refs.
Heat and mass transfers in the gas and solid phases			
Effective axial dispersion coefficient of the *k*-th substance in the gas phase	$\frac{1}{\mathrm{Pe}_z} = \frac{0.28}{\mathrm{Re}\cdot\mathrm{Sc}} + 0.25\left(1+\frac{1}{1+750\cdot\mathrm{Re}^{-2}}\right)+ 0.03\frac{E^2}{(1+E)}\cdot\frac{1}{(\mathrm{Re}\cdot\mathrm{Sc})^{-1}+0.5E^{1/2}},\ E = 4.2\mathrm{Re}^{-0.5}$	(12)	[38,39]
Effective axial thermal conductivity coefficient in the solid phase	$\lambda^e = \lambda_g\cdot(7+B\mathrm{Re}_m\mathrm{Pr})$	(13)	[38,40,41]
Internal mass transfer			
Knudsen diffusion coefficient	$D_K = 97r_p\sqrt{\frac{T_{ref}}{M}}$	(14)	[42]
Effective diffusion coefficient for the de-N_2O catalyst	$D_c^e = P_e\left(\frac{1}{D_m}+\frac{1}{D_K}\right)^{-1}$	(15)	[42]
Effectiveness factor for the de-N_2O catalystObserved reaction rate of de-N_2O	$\eta = \left(\frac{3}{\psi}\right)\cdot\left[\left(\frac{1}{th(\psi)}\right)-\frac{1}{\psi}\right],\ \psi = \frac{d_p}{2}\cdot\sqrt{\frac{k}{D_c^e}}$	(16)	
	$W = \eta\cdot k\cdot C_{N_2O}$	(17)	
External heat and mass transfers			
Sherwood number	$\mathrm{Sh} = 0.395\mathrm{Re}_m^{0.64}\cdot\mathrm{Sc}^{1/3}$	(18)	[38]
Nusselt number	$\mathrm{Nu} = 0.395\mathrm{Re}_m^{0.64}\cdot\mathrm{Pr}^{1/3}$	(19)	[38]
Pressure drop and catalyst loading			
Pressure drop along the bed	$\Delta P = H\cdot\left[150\frac{(1-\varepsilon)^2}{\varepsilon^3}\cdot\frac{\mu\cdot u}{{d_p}^2}+1.75\frac{(1-\varepsilon)}{\varepsilon^3}\cdot\frac{\rho\cdot u^2}{d_p}\right]$	(20)	[38,43]
Catalyst loading	$G = V\cdot\gamma$	(21)	

Table 6. Catalyst dimensions, stoichiometric equations, enthalpies, and kinetic equations.

Bed	Catalyst	Reaction	Kinetic Equation
SCR	V/Al, Cylinders, 5 × 15 mm	$NH_3 + NO + 0.25O_2 \rightarrow N_2 + 1.5H_2O$, $(-\Delta H_{SCR})$ = 407 kJ/mol	$W_{SCR} = k\cdot C_{NO_x}$
de-N_2O	$Cs/Ni_{0.1}Co_{2.9}O_4$, Cylinders, 3 × 5.2 mm	$N_2O \rightarrow N_2 + 0.5O_2$, $(-\Delta H_{N_2O})$ = 81 kJ/mol	$W_{N_2O} = k\cdot C_{N_2O}$

To estimate the kinetic parameters, we used the Levenberg–Marquardt optimization method [46,47] implemented in the COMSOL Multiphysics package. To determine the kinetic constants at different temperatures, the experimental data were approximated using an isothermal plug-flow model.

Thermophysical and thermodynamic parameters, coefficients of axial heat and mass transfers, as well as interphase heat and mass exchange values (Table 5), were calculated at the reference temperature. For solving the system of partial differential equations with appropriate boundary conditions (1)–(8), we used the COMSOL Multiphysics package, which is a common tool for modeling catalytic reactors [48–51].

4.3. Input Data for the Calculations

The mathematical modeling of the process was performed by varying the inlet parameters in the ranges that are common in industrial UKL plants:

- Inlet temperature (T_g^{in}): 230–270 °C;

- Gas flow rate (Q): 46,040–58,670 m^3/h (STP), which corresponds to the linear velocity of 1.128–1.437 m/s.

Fixed values:

- Reactor diameter: 3.8 m;
- Gas composition at the inlet to the first bed (vol.%): NO_x—0.15, NH3—0.165, N_2O—0.15, oxygen—5, water—2, and nitrogen—by balance;
- Working pressure: 0.716 MPa.

As a result of modeling, catalyst loading using layers was determined to provide the target degree of NO_x and N_2O removal from the tail gas, as mentioned below; the calculations were performed taking into account the following restrictions:

- The catalyst bed height (H) should not exceed the maximum allowable space according to the UKL plant's catalytic purification reactor design: 0.5 m for SCR, 0.7 m for de-N_2O [5,6];
- The maximum temperature in the SCR catalyst bed (Tmax) should not exceed 280 °C because the selectivity of aluminum–vanadium catalysts decreases at a higher temperature;
- The emissions of NO_x and N_2O at the reactor outlet should be less than 50 ppm, which, at the preset inlet concentrations of nitrogen oxides, corresponds to a conversion rate of not less than 98%.

The total pressure drop in the reactor was also calculated based on the obtained bed heights.

5. Conclusions

Our experimental studies of N_2O decomposition on a $Cs/Ni_{0.1}Co_{2.9}O_4$ catalyst in an isothermal flow reactor within a temperature range of 160–250 °C proved that a N_2O conversion rate of up to 95–99% could be obtained at a residence time of 0.6–0.8 s. The reaction rate constants k_0 = 7.23·10^8 s^{-1} and E_a = 77.15 kJ/mol were determined and further used for modeling the process. Mathematical modeling allowed us to estimate the parameters of a commercial two-bed reactor for NO_x and N_2O low-temperature mitigation in a nitric acid plant to ensure that a residual content of each would be less than 50 ppm, under temperature and spatial constraints. The effect of inlet temperature and tail-gas flow rate on the degrees of conversion and catalyst bed heights was simulated. At the optimal inlet temperature of ~260 °C, the process can be performed in the widest range of tail-gas flow rates varying from 46,040 to 58,670 m^3/h.

Author Contributions: Software, formal analysis, investigation, writing—original draft preparation, N.V.; methodology, conceptualization, validation, and investigation, Y.I.; software, investigation, writing—original draft preparation, visualization, A.S.; methodology, conceptualization, supervision, writing—review and editing, V.C.; methodology, supervision, L.I. All authors have read and agreed to the published version of the manuscript.

Funding: This research was funded by the Ministry of Science and Higher Education of the Russian Federation within the governmental order for the Boreskov Institute of Catalysis (projects AAAA-A21-121011490008-3, AAAA-A21-121011390010-7).

Data Availability Statement: Not applicable.

Conflicts of Interest: The authors declare no conflict of interest.

Nomenclatures

B	Constant (0.0643);
$C_{NO_x(N_2O)}$	Concentration of NO_x (N_2O), mol/m^3;
c_p	Gas heat capacity, J·m^{-3}·K^{-1};
d_p	Catalyst diameter, mm;

D_K	Knudsen diffusion coefficient, m^2/s;
D	Diffusion coefficient, m^2/s;
D_m	Coefficient of molecular diffusion, m^2/s;
E_a	Activation energy, J/mol;
G	Catalyst loading, kg;
$(-\Delta H_j)$	Enthalpy of *j-th* reaction, J/mol;
H	Catalyst bed height, m;
k_0	Pre-exponential factor, s^{-1};
k	Rate constant, s^{-1};
M	Molecular weight of N_2O, g/mol;
P	Pressure, Pa;
P_0	Pressure at STP, Pa;
ΔP	Pressure drop, Pa;
P_e	Catalyst permeability;
Q	Volumetric flow rate, m^3/h;
r_p	Pore radius, m;
S_{sp}	Specific surface area, m^{-1};
T	Temperature, K;
T_0	Temperature at STP, K;
T_{ref}	Reference temperature, K;
ΔT_{ad}	Adiabatic temperature, K;
u_0	Linear velocity at STP, m/s;
V	Catalyst volume, m^3;
V_m	Molar volume at STP, m^3/mol;
W	Rate of reaction, $mol \cdot m^{-3} \cdot s^{-1}$;
X	Conversion,%;
y_i	Concentration of *i*-th component, mole fraction;
z	Axial coordinate, m.
Greek letters:	
α	Coefficient of heat exchange, $W \cdot m^{-2} \cdot K^{-1}$;
β	Coefficient of mass exchange, m/s;
γ	Bulk density, kg/m^3;
ε	Porosity;
η	Effectiveness factor;
λ	Thermal conductivity, $W \cdot m^{-1} \cdot K^{-1}$;
μ	Dynamic viscosity, $kg \cdot m^{-1} \cdot s^{-1}$;
ν_i	Stoichiometric coefficients;
τ	Residence time, s;
ψ	Thiele modulus.
Subscripts:	
c	Catalyst;
g	Gas;
max	Maximum value.
Superscripts:	
e	Effective value;
in	Inlet;
out	Outlet.
Dimensionless groups:	
Nu	Nusselt number;
Pe	Peclet number;
Pr	Prandtl number;
Re	Reynolds number;
Re_m	Modified Reynolds number;
Sc	Schmidt number;
Sh	Sherwood number.

References

1. Pérez-Ramirez, J.; Kapteijn, F.; Schöffel, K.; Moulijn, J.A. Formation and control of N_2O in nitric acid production: Where do we stand today? *Appl. Catal.* **2003**, *44*, 117–151. [CrossRef]
2. Boll, W. Prolonged campaign length of high pressure nitric acid plant by optimization of secondary catalyst design for N_2O abatement. In Proceedings of the Int. Conf. & Exhib Nitrogen+Syngas 2017, London, UK, 27 February 2017.
3. Groves, M.C.E.; Sasonow, A. Uhde EnviNO$_x$® technology for NO_X and N_2O abatement: A contribution to reducing emissions from nitric acid plants. *J. Integr. Environ. Sci.* **2010**, *7*, 211–222. [CrossRef]
4. EPA December 2010. Available and Emerging Technologies for Reducing Greenhouse Gas Emissions from Nitric Acid Production Industry. Available online: https://www.epa.gov/sites/production/files/2015-12/documents/nitricacid.pdf (accessed on 13 January 2023).
5. Chumachenko, V.A.; Isupova, L.A.; Ivanova, Y.A.; Ovchinnikova, E.V.; Reshetnikov, S.I.; Noskov, A.S. Technologies for Simultaneous Low-Temperature Catalytic Removal of NO_x and N_2O from the Tail Gases of Nitric Acid Plants. *Chem. Sustain. Dev.* **2020**, *28*, 203–212. [CrossRef]
6. Chumachenko, V.A.; Zenkovets, G.A.; Shutilov, A.A.; Kharitonov, A.S.; Pirutko, L.V.; Mokrinsky, V.V.; Noskov, A.S. Low-temperature abatement of nitrogen oxides (NO_x, N_2O) from the effluent gases in nitric acid production. In Proceedings of the XIX Int. Conf. on Chemical Reactors (CHEMREACTOR-19), Vienna, Austria, 5 September 2010.
7. Zenkovets, G.A.; Shutilov, A.A.; Ivanova, G.G.; Slavinskaya., E.M.; Chumachenko, V.A.; Noskov, A.S. Catalyst, method of its preparation and method of purification of tail gases from nitrogen oxides. Patent RU 2647847 C1, 22 May 2017.
8. Kladova, N.V.; Borisova, T.V.; Makarenko, M.G.; Chumachenko, V.A. Aluminum-vanadium catalyst for selective purification from nitrogen oxides with ammonia and method for its production. Patent RU 2167708 C1, 3 March 2000.
9. Yu, H.; Wang, X. Apparent activation energies and reaction rates of N_2O decomposition via different routes over Co_3O. *Catal. Commun.* **2018**, *106*, 40–43. [CrossRef]
10. Kapteijn, F.; Marban, G.; Rodriguez-Mirasol, J.; Moulijn, J.A. Kinetic Analysis of the Decomposition of Nitrous Oxide over ZSM-5 Catalysts. *J. Catal.* **1997**, *167*, 256–265. [CrossRef]
11. Dandl, H.; Emig, G. Mechanistic approach for the kinetics of the decomposition of nitrous oxide over calcined hydrotalcites. *Appl. Catal. A Gen.* **1998**, *168*, 261–268. [CrossRef]
12. Isupova, L.A.; Ivanova, Y.A. Removal of nitrous oxide in nitric acid production. *Kinet. Catal.* **2019**, *60*, 744–760. [CrossRef]
13. Konsolakis, M. Recent advances on nitrous oxide (N_2O) decomposition over non–noble metal oxide catalysts: Catalytic performance, mechanistic considerations and surface chemistry aspects. *ACS Catal.* **2015**, *5*, 1–87. [CrossRef]
14. Yu, H.; Qi, X.; Du, X.; Pan, Y.; Feng, X.; Shan, W.; Xiong, Y. The preparation of 3.0F-Co_3O_4 catalyst with "Yardang Landform" structure and its performance for catalyzing N_2O decomposition. *Mol. Catal.* **2023**, *537*, 112960. [CrossRef]
15. Choi, S.; Nam, K.B.; Ha, H.P.; Kwon, D.W. Enhancement of Catalytic N_2O Decomposition by Modulating Oxygen Vacancies over Cu/Ce1-XYX Catalysts. *J. Ind. Eng. Chem.* 2023; *in press*. [CrossRef]
16. Qi, J.; Qi, X.; Pan, Y.; Cui, J.; Xiong, Y.; Shan, W.; Yu, H. Sm doped NiO catalysts with excellent H_2O resistance for N_2O decomposition under simulated nitric acid plant exhaust condition. *Appl. Surf. Sci.* **2023**, *611*, 155657. [CrossRef]
17. Klegova, A.; Pacultova, K.; Kiska, T.; Peikertova, P.; Rokicinska, A.; Kustrowski, P.; Obalova, L. Washcoated open-cell foam cobalt spinel catalysts for N_2O decomposition. *Mol. Catal.* **2022**, *533*, 112754. [CrossRef]
18. Xiong, Y.; Zhao, Y.; Shan, W.; Feng, X.; Cui, J.; Lou, Z.; Shao, G.; Dong, M.; Yu, H. Potassium promoted $Gd_{0\cdot06}Co$ catalysts for highly efficient catalytic N_2O decomposition in presence of impurity gases at low temperature. *Chemosphere* **2022**, *303*, 135257. [CrossRef]
19. Ma, Z.; Ren, Y.; Lu, Y.B.; Peter, P.G. Catalytic decomposition of N_2O on ordered crystalline metal oxides. *J. Nanosci. Nanotechnol* **2013**, *13*, 5093–5103. [CrossRef]
20. Hu, X.; Wang, Y.; Wu, R.; Zhao, Y. Graphitic carbon nitride-supported cobalt oxides as a potential catalyst for decomposition of N_2O. *Appl. Surf. Sci.* **2021**, *538*, 148157. [CrossRef]
21. Yan, L.; Ren, T.; Wang, X.; Ji, D.; Suo, J. Catalytic decomposition of N_2O over $M_xCo_{1-x}Co_2O_4$ (M = Ni, Mg) spinel oxides. *Appl. Catal. B Env.* **2003**, *45*, 85–90. [CrossRef]
22. Liu, Z.; He, F.; Ma, L.; Peng, S. Recent Advances in Catalytic Decomposition of N_2O on Noble Metal and Metal Oxide. *Catal. Catal. Surv. Asia* **2016**, *20*, 121–132. [CrossRef]
23. Zheng, L.; Li, H.-J.; Xu, X.-F. Catalytic decomposition of N_2O over Mg-Co composite oxides hydrothermally prepared by using carbon sphere as template. *J. Fuel Chem. Technol.* **2018**, *46*, 569–577. [CrossRef]
24. Zhang, H.-J.; Wang, J.; Xu, X.-F. Catalytic decomposition of N_2O over $Ni_xCo_{1-x}CoAlO_4$ spinel oxides prepared by sol-gel method. *J. Fuel Chem. Technol.* **2015**, *43*, 81–87. [CrossRef]
25. Russo, N.; Fino, D.; Saracco, G.; Specchia, V. N_2O catalytic decomposition over various spinel-type oxides. *Catal. Today* **2007**, *119*, 228–232. [CrossRef]
26. Abu-Zied, B.M.; Soliman, S.A.; Abdellah, S.E. Pure and Ni-substituted Co_3O_4 spinel catalysts for direct N_2O decomposition. *Chin. J. Catal.* **2014**, *35*, 1105–1112. [CrossRef]
27. Krezhov, K.; Konstantinov, P. Cationic distributions in the binary oxide spinels $M_xCo_{3-x}O_4$ (M = Mg,Cu,Zn,Ni). *Phys. B Cond. Matter* **1997**, *234–236*, 157–158. [CrossRef]

28. Wójcik, S.; Grzybek, G.; Stelmachowski, P.; Sojka, Z.; Kotarba, A. Bulk, Surface and Interface Promotion of Co_3O_4 for the Low-Temperature N_2O Decomposition Catalysis. *Catalysts* **2020**, *10*, 41. [CrossRef]
29. Stelmachowski, P.; Maniak, G.; Kotarba, A.; Sojka, Z. Strong electronic promotion of Co_3O_4 towards N_2O decomposition by surface alkali dopants. *Catal. Commun.* **2009**, *10*, 1062–1065. [CrossRef]
30. Maniak, G.; Stelmachowski, P.; Kotarba, A.; Sojka, Z.; Rico-Pérez, V.; Bueno-López, A. Rationales for the selection of the best precursor for potassium doping of cobalt spinel based de-N_2O catalyst. *Appl. Catal. B Env.* **2013**, *136–137*, 302–307. [CrossRef]
31. Ivanova, Y.A.; Ivanov, D.A.; Chumachenko, V.A.; Isupova, L.S.; Noskov, A.S. One-reactor scheme for NO and N_2O low-temperature abatement from tail gas in nitric acid production. In Proceedings of the XXII International Conference on Chemical Reactors (CHEMREACTOR-22), London, UK, 19 September 2016.
32. Ivanova, Y.A.; Sutormina, E.F.; Isupova, L.A. Low-temperature decomposition of nitrous oxide in the presence of 1%Cs/MgxCo3–xO4 (x = 0–0.9) Oxides. *Kinet. Catal.* **2020**, *61*, 646–653. [CrossRef]
33. Ivanova, Y.A.; Sutormina, E.F.; Isupova, L.A.; Rogov, V.A. Effect of the Composition of $Ni_xCo_{3-x}O_4$ (x = 0–0.9) Oxides on Their Catalytic Activity in the Low-Temperature Reaction of N_2O Decomposition. *Kinet. Catal.* **2018**, *59*, 357–362. [CrossRef]
34. Obalová, L.; Jirátová, K.; Karásková, K.; Kovanda, F. Simulation of N_2O abatement in waste gases by its decomposition over a K-promoted Co-Mn-Al mixed oxide catalyst. *Chin. J. Catal.* **2011**, *32*, 816–820. [CrossRef]
35. Walter, S.; Malmberg, S.; Schmidt, B.; Liauw, M.A. Mass transfer limitations in microchannel reactors. *Catal. Today* **2005**, *110*, 15–25. [CrossRef]
36. Rossetti, I. Continuous flow (micro-) reactors for heterogeneously catalyzed reactions: Main design and modelling issues. *Catal. Today* **2018**, *308*, 20–31. [CrossRef]
37. Perez-Ramires, J.; Berger, R.J.; Mul, G.; Kapteijn, F.; Moulijn, J.A. The six-flow reactor technology. *A review on fast catalyst screening and kinetic studies, Catal. Today* **2000**, *60*, 93–109. [CrossRef]
38. Aerov, M.E.; Todes, O.M.; Narinsky, D.A. *Apparatuses with a Stationary Granular Beds*, 1st ed.; Khimiya: Leningrad, Russia, 1979; pp. 1–176.
39. Ovchinnikova, E.V.; Vernikovskaya, N.V.; Gribovskii, A.G.; Chumachenko, V.A. Multichannel microreactors for highly exothermic catalytic process: The influence of thermal conductivity of reactor material and of transport phenomena inside the channels on the process efficiency. *Chem. Eng. J.* **2021**, *409*, 128046. [CrossRef]
40. Yagi, S.; Wakao, N. Heat and mass transfer from wall to fluid in packed beds. *AIChE J.* **1959**, *5*, 79–85. [CrossRef]
41. Yagi, S.; Kunii, D.; Wakao, N. Studies on axial effective thermal transfer conductivities in packed beds. *AIChE J.* **1960**, *6*, 543–546. [CrossRef]
42. Salmi, T.O.; Mikkola, J.-P.; Warna, J.P. *Chemical Reaction Engineering and Reactor Technology*, 1st ed.; CRC Press: Boca Raton, FL, USA, 2010; pp. 1–638.
43. Bird, R.B.; Stewart, W.E.; Lightfoot, E.N. *Transport Phenomena*, 2nd ed.; John Wiley & Sons: New York, NY, USA, 2002; pp. 1–897.
44. Ovchinnikova, E.V.; Chumachenko, V.A.; Piryutko, L.V.; Kharitonov, A.S.; Noskov, A.S. Neutralization of nitrous gases in the production of adipic acid: Technology of two-stage catalytic purification. *Catal. Ind.* **2009**, *1*, 76–84. [CrossRef]
45. Pavlenko, N.I. Low-Temperature Catalytic Waste Gases Purification in the Production of Nitric Acid. Bachelor's Thesis, NSTU, Novosibirsk, Russia, 2018.
46. Klegovà, A.; Pacultovà, K.; Fridrichovà, D.; Volodarskaya, A.; Kovanda, F.; Jiratovà, K. Cobalt oxide catalysts on commercial supports for N_2O decomposition. *Chem. Eng. Technol.* **2017**, *40*, 981–990. [CrossRef]
47. Tian, P.; Yu, Z.; Yuan, Y. A smoothing Levenberg-Marquardt algorithm for linear weighted complementarity problem. *AIMS Math.* **2023**, *8*, 9862–9876. [CrossRef]
48. Chen, L.; Ma, Y. A New Modified Levenberg–Marquardt Method for Systems of Nonlinear Equations. *J. Math.* **2023**, *2023*, 6043780. [CrossRef]
49. Wei, S.; Li, C. Design and optimization of spiral heated tubular dimethyl ether (DME) steam reforming reactor. *Int. J. Hydrog. Energy* **2023**, *48*, 2231–2246. [CrossRef]
50. Zazhigalov, S.; Elyshevb, A.; Zagoruiko, A. Catalytic reverse-flow oxidation process in reactors of various designs: Axial, side and tangential gas inlet. *Chem. Eng. Res. Des.* **2023**, *191*, 364–374. [CrossRef]
51. Vernikovskaya, N.V.; Sheboltasov, A.G.; Ovchinnikova, E.V.; Gribovskiy, A.G.; Chumachenko, V.A. Experimental and theoretical investigation of the oxidation of methanol to formaldehyde in a microstructured slit-type catalytic reactor. *Chem. Eng. J.* **2023**, *451*, 138368. [CrossRef]